Korean J. Chem. Eng., 35(8), 1756-1763 (2018)
DOI: 10.1007/s11814-018-0073-1

pISSN: 0256-1115
eISSN: 1975-7220

Preparation of graphene aerogel-poly(3,4-ethylenedioxythiophene) conductive composite by using simultaneous co-vaporized vapor phase polymerization

Kerguelen Mae Nodora and Jin-Heong Yim†

Division of Advanced Materials Engineering, Kongju National University,
Budaedong 275, Seobuk-gu, Cheonan-si, Chungnam 31080, Korea
(*Received 8 March 2018 • accepted 2 May 2018*)

Abstract−We prepared spherical reduced graphene oxide aerogels (rGOA) through freeze casting and thermal reduction for the fabrication of carbon-conducting polymer composites with excellent electrical and mechanical properties. The rGOA-poly(3,4-ethylenedioxythiophene) (PEDOT) or rGOA-PEDOT-SiO_2 composites were prepared by simultaneous co-vaporized vapor phase polymerization (SC-VPP). The rGOA spherical particles, prepared by freeze casting of GO solution, had a radially oriented pore structure at the center of its cross section and increasing density of GO sheet towards its center because the temperature gradient of the droplet of the GO solution rapidly freezes from the water outside the droplet during the process. The morphology of the rGOA-PEDOT-SiO_2 composites prepared using SC-VPP was more spherical compared to rGOA-PEDOT composites, and the orientation of the cross-pore structure was well-developed. Moreover, micrometer-sized conductive PEDOT-SiO_2 hybrid spheres could be formed on the composite's surface by controlling the amount of FTS oxidant. The rGOA-PEDOT-SiO_2 composites showed lower resistance values and higher current densities at the same voltage than rGOA or rGOA-PEDOT composites. This can be attributed to the surface area of the particle's surface, which is enlarged due to the presence of the microspheres, which can cause the widening of the contact area with the electrode to facilitate better electron migration.

Keywords: Conducting Polymer, PEDOT, Graphene Aerogel, Simultaneous Co-vaporized Vapor Phase Polymerization, Electrical Property

INTRODUCTION

Graphene, which has a hexagonal lattice structure and is shaped like a honeycomb with carbon atoms, has excellent physical properties in terms of electrical conductivity as well as mechanical strength and thermal conductivity. Therefore, it has been applied to various fields since its introduction in 2004 [1,2]. Typically, graphene is capable of mass production of graphene oxide (GO) dispersed by the exfoliation of graphite expanded by Hummer's method [3]. The GO can be chemically or thermally reduced, and reduced graphene oxide (rGO) with high electrical conductivity can be obtained. rGO has excellent electrical properties, but aggregation of rGO frequently occurs because of the van der Waals force between them. To address these problems, many studies have been made for uniform dispersion of various solvents or polymers by controlling the functional group of the graphene [4-6]. Graphene aerogel (GA) have been attracting much interest in its synthesis and application [7-9]. GA is formed by a porous conductive network and is widely used in environment and energy applications such as adsorption, composite, electrode, and sensor materials [10,11]. GA is prepared by freezing the GO dispersed aqueous solution under liquid nitrogen and preparing graphene oxide aerogel (GOA) by the formation of interconnected pore skeletons during the self-assembly and freeze-drying process of the GO sheet [12]. GOA is chemically or thermally reduced to produce reduced graphene oxide aerogels (rGOA) with high electrical conductivity. Generally, the pore wall of GA is composed of lamination of a very thin and flexible GO sheet, and it has the same properties as an elastic body with excellent restoring force against external stress. However, GA has been combined with other polymers or carbon materials as composites to improve its performance since it does not have sufficient mechanical strength and chemical stability required for various applications [13-15]. For example, the carbon nanotube (CNT) composited with rGOA, in which the CNT skeleton is embedded in the pore wall, exhibits a large volume of elastic volume recovery after compression compared to the plastic deformation found in rGOA [13]. In addition, the composite made by coating the rGOA with an organic polymer served as a compressive-resistant supercapacitor electrode with improved specific capacitance [14,15].

Researches on conductive polymers such as poly (3,4-ethylenedioxythiophene) (PEDOT), polypyrrole (PPy) and polyaniline (PANi) have been continuously ongoing since the discovery of polyacetylene [16]. Researches have been reported also on improving the performance of devices in the energy field by combining such conductive polymers with rGOA materials [14,15,17]. A. Ouyang et al. demonstrated rGOA-PANi spherical composites, which form a sandwiched pore wall structure by depositing PANi electrochemically on rGOA and coating it with a soft PANi layer on both sides of the GO sheet, which constitutes the framework of the pore structure of rGOA [17]. These rGOA-PANi spherical composites showed

†To whom correspondence should be addressed.
E-mail: jhyim@kongju.ac.kr

improved specific capacitance up to 669 F/g and excellent cycle stability. The hybridization of the conductive polymer with the organic-inorganic material can be variously carried out by the wet process [18,19]. In recent years, we have been studying organic-inorganic hybrid materials using vapor phase polymerization [20-26]. In particular, simultaneous co-vaporized vapor phase polymerization (SC-VPP) can produce homogeneous multifunctional organic-inorganic composite at the molecular level, which cannot be achieved by simple solution-solution or solid-solution mixing. When SC-VPP is carried out, the monomer in the gaseous phase easily embeds itself on the interface of the solid, and the polymerized layer can be uniformly formed, so that coating on various substance having complex shapes is easy [24,25,27-29].

In this study, rGOA spheres were prepared by freeze casting and thermal reduction and then carbon-conductive polymer spherical composites (rGOA-PEDOT or rGOA-PEDOT-SiO_2) with excellent electrical and mechanical properties were fabricated *via* VPP. The morphology, chemical composition and pore structure of rGOA and rGOA-PEDOT or rGOA-PEDOT-SiO_2 spherical composites were compared and analyzed. In addition, electrical characteristics such as threshold voltage, electrical resistance, and specific capacitance of various rGOA-PEDOT or rGOA-PEDOT-SiO_2 spherical composites were investigated.

MATERIALS AND METHODS

1. Chemicals

3,4-Ethylenedioxythiophene (EDOT, MD Bros.) as monomer for PEDOT, iron (III) *p*-toluenesulfonate (FTS, ALDRICH) as oxidant and dopant and 1-butanol (JUNSEI, Japan) as solvent were used without further purification. Graphene oxide solution (5 g/L, GO-A400, GRAPHENE ALL, Korea) and sodium carboxymethyl cellulose (SCC, ALDRICH) were used for the preparation of GOA spherical particles. Ethanol (ALDRICH) was used for washing unreacted reactants after preparation of rGOA-PEDOT hybrid spherical composites. Tetraethyl orthosilicate (TEOS, SAMCHUN, Korea) was used as a monomer of SiO_2 without purification as well.

2. Preparation of GOA Spherical Particles

SCC with a concentration of 1 wt% was dissolved in 10 ml of a GO water dispersion solution (5 g/L) as a binder of the particles. The completely dissolved aqueous solution of GO and SCC was transferred in a 3 ml syringe (needle diameter: 0.7 mm). The GO water dispersion was slowly added in a dropwise manner to the low temperature beaker filled with liquid nitrogen by a needle syringe (Scheme 1(a)). The contents in the low temperature beaker were then placed in a 100 ml flask to be freeze-dried with liquid nitrogen. The flask was kept at 0 °C and vacuum-dried for 4 h using a vacuum pump (Scheme 1(b)). The obtained GOA spherical particles were placed in a crucible and thermally reduced in a furnace at 400 °C for 5 min to produce rGOA spherical particles having a diameter of 1 to 2 mm (Scheme 1(c)).

3. Preparation of r-GOA-PEDOT Hybrid by SC-VPP

The rGO-PEDOT or rGOA-PEDOT-SiO_2 spherical composites were prepared *via* SC-VPP. The oxidizing agent, FTS, was added in amounts of 10, 20 and 30 wt% with 1-butanol in three beakers, respectively, and completely dissolved by stirring. After 0.1 g of spherical particles of rGOA were immersed in the prepared FTS solution (10, 20, 30 wt%) for 30 min (Scheme 2(b)), the beakers were then ultra-sonicated to let the FTS penetrate toward the inner pore of rGOA (Power Sonic 410, Hwasin Tech). After the FTS

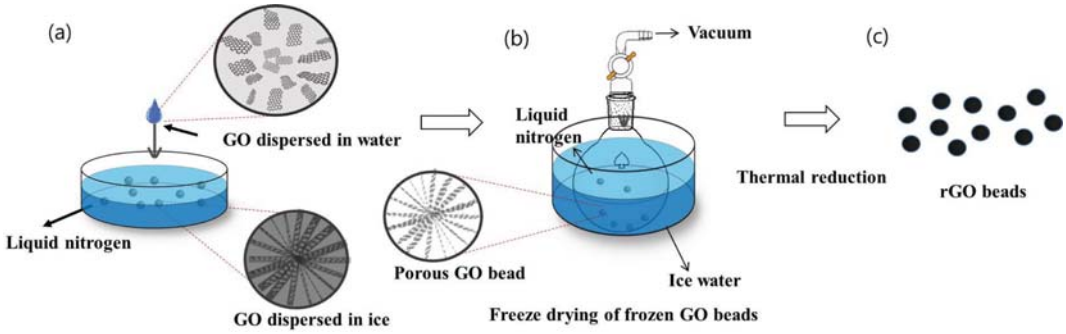

Scheme 1. Systematic preparation scheme of GOA and rGOA spherical particles.

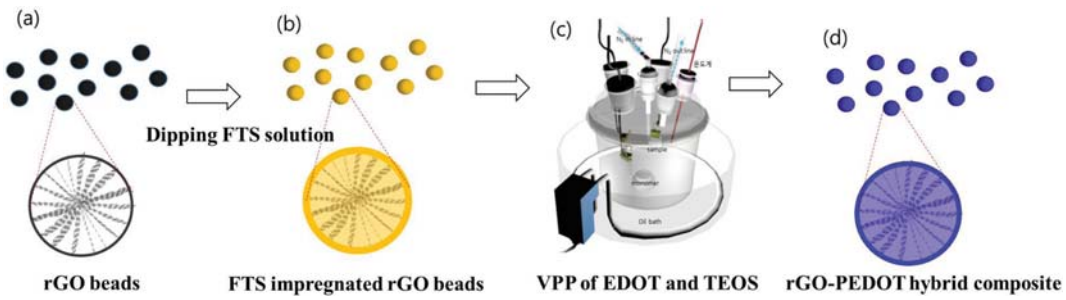

Scheme 2. Preparation route of rGOA-PEDOT, rGOA-PEDOT-SiO_2 composite.

Table 1. The atomic content of sulfur and silicon in the rGOA-PEDOT hybrid material as a function of FTS content[a]

FTS contemt (wt%)	rGOA-PEDOT hybrid		rGOA-PEDOT-SiO_2 hybrid	
	S (atomic %)	Si (atomic %)	S (atomic %)	Si (atomic %)
10	3.06	-	3.00	1.27
20	4.33	-	3.05	1.40
30	6.96	-	3.16	8.02

[a]S at% of rGO=2.29, Si at% of rGO=0.14

impregnated rGOA, it was then moved into the mesh pocket in the VPP reactor after drying for 10 min in an oven at 60 °C (Scheme 2(c)). The conductive monomer (EDOT) was also placed in the petri dish at the bottom of the VPP reactor. The inside of the reactor was charged with nitrogen at a flow rate of 10 mL/s for 30 min before the polymerization to suppress the recrystallization of FTS. The PEDOT polymerization was carried out at 60 °C for 30 min. EDOT and TEOS were mixed at a weight ratio of 1 : 1 and placed in a petri dish at the bottom of the reactor for the preparation of rGOA-PEDOT-SiO_2 spherical composite with improved mechanical properties. After the polymerization for 30 min, it was immersed in ethanol for at least 1 h and then separated using a filtrating apparatus. The prepared hybrid particle was dried in an oven at 60 °C.

4. Characterization of PEDOT-graphene Hybrid Composite

The surface and cross section of rGOA, rGOA-PEDOT or rGOA-PEDOT-SiO_2 spherical particles were observed using a scanning electron microscope (SEM, TESCAN, VEGA3) to confirm the morphological characteristics. Fourier-transform infrared spectroscopy (FT-IR, Thermo Scientific, NICOLET 6700) was performed with the resolution of 4 cm^{-1} from 4,000 to 500 cm^{-1} to investigate the thermal reduction of the GOA into the particle form to rGOA. Energy dispersive X-ray spectroscopy (EDS, BRUKER, X FLASH, U.S.A.) and X-ray photoelectron spectroscopy (XPS, MultiLab, ESCA 2000) were performed to analyze the chemical composition of spherical particles before and after polymerization. The XPS scans from 0 to 1,200 eV binding energy with 0.05 eV steps. A measuring device was prepared to investigate the electrical properties of the rGOA-PEDOT or rGOA-PEDOT-SiO_2 spherical particles. A silver line with a thickness of 200 to 250 nm was deposited on a glass substrate using a thermal evaporator. The deposited silver line and the hybrid spherical particles were connected by the same contact area using a silver paste to fabricate the measurement device (Fig. 8(a)). The device was connected to a power supply (EXSO®, DC power supply K6133A) using an LED bulb and electric wire to check the threshold voltage by gradually increasing the voltage until the lighting of the LED bulb. Specific capacitance and resistance values were measured in parallel mode after connecting the measurement devices and the LCR meter (GW INSTEK, LCR-6100). A current-voltage curve of a single spherical particle was obtained in an E526× E5270B IV sweep mode at a voltage range of 0 to 10 V using a probe

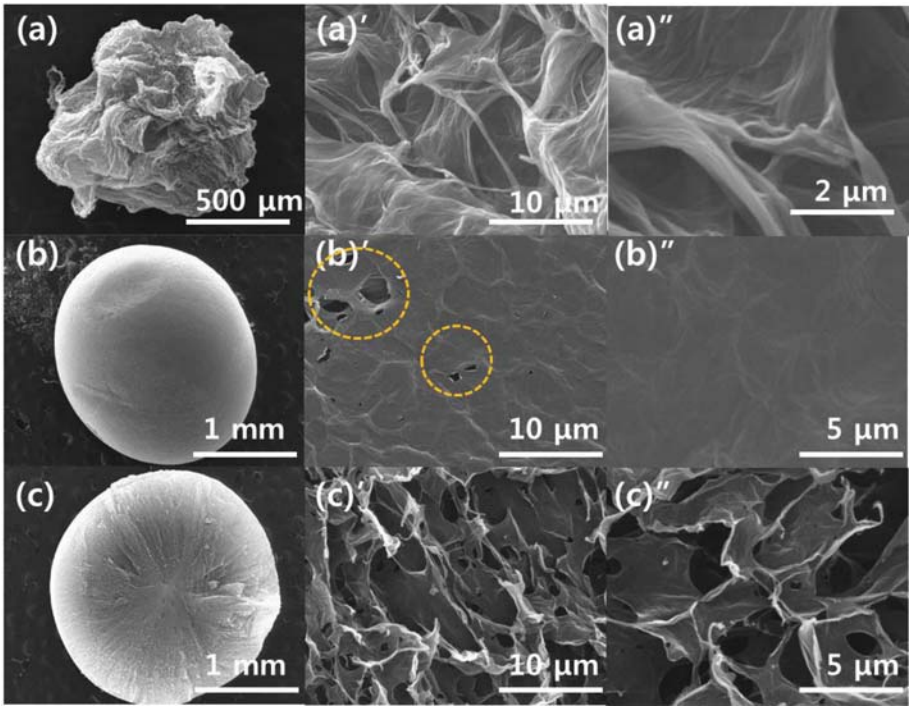

Fig. 1. Morphology of GO and GO bead (a), (a)′, (a)″ SEM image of GOA beads prepared without SCC, SEM of image (b), (b)′, (b)″ surface images, (c), (c)′, (c)″ cross sectional images.

station (Agilent Technologies, E5270A).

RESULTS AND DISCUSSION

1. Physico-chemical Structure Analysis of rGOA-PEDOT Hybrid Composite

In this study, we used the freeze casting method (Scheme 1(a)), which can be used to fabricate porous materials such as graphene [12,17], ceramic [30] or organic polymers [31,32], to prepare GOA sphere particle having microporous structure. Subsequently, rGOA spheres were prepared by using a thermal reduction process (Scheme 1(b)). Unlike the results of the method which employs the dropping of GO aqueous solution into liquid nitrogen by Ouyang et al. [17], GOA spherical particles could not be formed due to insufficient cohesion between GO sheets in our experimental conditions (Fig. 1(a)). However, it was possible to make spherical particles with uniform surface (Fig. 1(b)), when 1 wt% of SCC, a natural polymer, was added to the aqueous solution of GO and freeze-casting the aqueous mixture. The morphology of the surface of the rGOA spherical particles has a smooth shape due to the reduced GO sheets forming a film as shown in Fig. 1(b)′ and (b)″. Unlike the surface morphology of the GOA particles reported in the literature [17], the pores were almost closed on the surface and only a part of the graphene was torn (Fig. 1(b)′, inside the yellow circle). It is hypothesized that this is because the SCC that was used as binder also acts as a stabilizer at the interface between GO and water. The radial pore channels from the spherical center to the surface can be clearly distinguished from the cross section of the GOA (Fig. 1(c), (c)′). This is consistent with the results reported in previous papers [12,17]. The reason for this morphology is that during the freeze casting, the GO solution is supplied with water droplets, so that immediately after the liquid nitrogen is locked and surrounded, each water droplet is subjected to a large temperature gradient. This temperature difference is created as an open hole that connects the radial channels by promoting the growth of ice crystals from the spherical surface toward the center. Liquid nitrogen causes the water to be rapidly cooled in the GO droplet. Afterwards, the frozen water was then eliminated during vacuum drying process, resulting in porous GOA sphere having a micrometer-sized pore. Fig. 2 shows the results of FT-IR analysis to confirm the

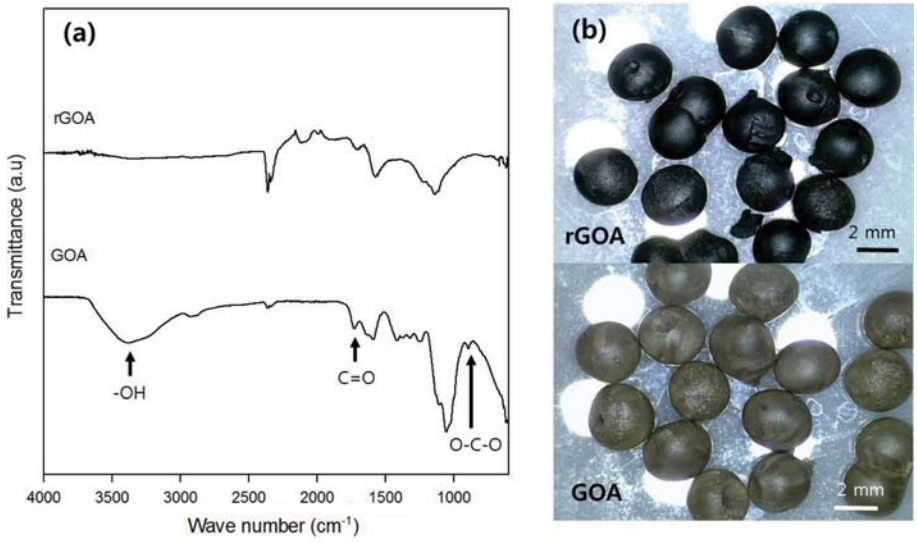

Fig. 2. Comparison of (a) FT-IR curves of GO and rGO bead (b) optical images of GO and rGO bead.

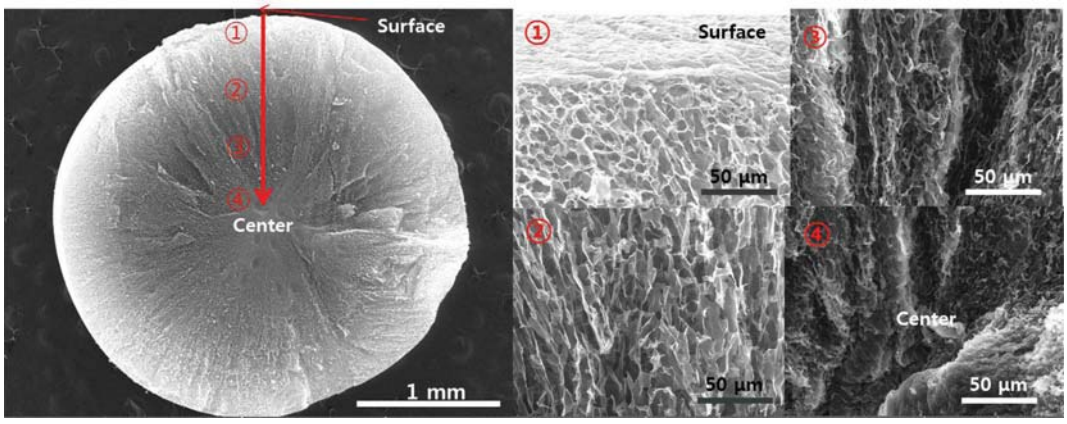

Fig. 3. Morphology changes of cross section for rGO bead as a function of radial direction.

chemical reduction of GOA to rGOA. In GOA, the peaks of 3,338 cm^{-1}, 1,033 cm^{-1} and 1,716 cm^{-1} corresponding to the functional groups of -OH, C-O-C and C=O were clearly observed. On the other hand, after the heat treatment at 400 °C the -OH and C-O-C group in rGOA disappeared as well as reduction in the C=O peak, which is a good indication that the reduction has proceeded effectively. GOA has a light khaki color, whereas thermally reduced rGOA particles are black (Fig. 2(b)). Fig. 3 shows a more detailed view of the cross section of the rGOA spherical particles. Based on Fig. 3, as the cross-section of the rGOA is moved from surface (①) to center (④), the orientation of the pore is directed at the center of the spherical particle and the density of the GO sheet increases toward the center. This phenomenon is caused by the temperature gradient in the liquid droplet when GO aqueous solution is gradually added into liquid nitrogen. As the ice starts to freeze from the outside of the droplet, the GO sheets start to position themselves at the center and the pore orientation and density start to vary as well.

The rGOA spherical particles as well as the rGOA-PEDOT or rGOA-PEDOT-SiO_2 spherical composites were prepared *via* the VPP process (Scheme 2) for the fabrication of carbon-conductive polymer composites with excellent electrical and mechanical properties. The PEDOT-rGOA particles, which were prepared *via* FTS impregnation and VPP, were contracted and it showed distorted surface morphology compared to rGOA which has a spherical shape with smooth surface. This might be due to the surface and inner pores of the rGOA which is elastic and when under stress pores forms on the surface (Fig. 4(e)) while the density of the GO sheets in the cross section becomes higher (Fig. 4(h)). It is evident that brittle PEDOT was formed on rGOA by the VPP process.

Our previous studies reported that the mechanical strength of the PEDOT-SiO_2 hybrid 2D film is dramatically increased and that the skeletal structure becomes stable [21-23]. rGOA-PEDOT-SiO_2 composite were prepared using SC-VPP which simultaneously co-evaporates EDOT and TEOS. TEOS is a precursor of SiO_2 component in the hybrid rGOA-PEDOT-SiO_2 composite. It was done in order to maintain the shape and pore orientation structure of the rGOA's spherical particles during hybridization with PEDOT (Fig. 4(c), (i)). The rGOA-PEDOT-SiO_2 composite also exhibits relatively less shrinkage and retains its spherical shape (Fig. 4(c)) and maintains the orientation structure of the pores (Fig. 4(i)) compared to rGOA-PEDOT composite. Fig. 4(f) shows the surface morphology of the rGOA-PEDOT-SiO_2 composite. On the surface of the rGOA-PEDOT-SiO_2 composite, micrometer-sized spherical bumps, which are believed to be PEDOT-SiO_2 hybrids, have been developed. These micro bumps were also observed in the porous PEDOT-SiO_2 hybrid conductive micro particles recently reported by our group [33]. These micro bumps cause and increase in the surface area of the porous conductive particles, thereby improving the electrical conductivity and specific capacitance of one particle. The surface morphology of the rGOA-PEDOT-SiO_2 composites prepared by increasing the amount of FTS oxidant in the SC-VPP process was investigated to control the amount of micro bumps. At 10 wt% of FTS, the surface of the rGOA particles, which were then flat before, was changed to the crushed rGOA-PEDOT-SiO_2 composite, in which no micro bumps were observed on the surface morphology. However, for the surface of the composite prepared using FTS 20 and 30 wt%, the size and number of bumps increase as the content of oxidizing agent increases.

EDS analysis was performed to compare the chemical composi-

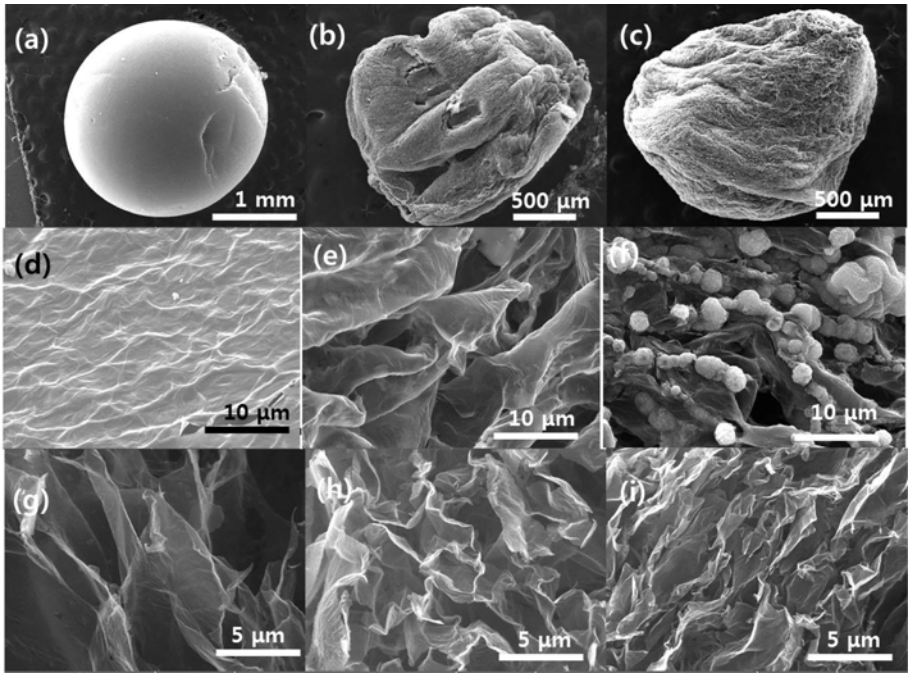

Fig. 4. Morphology of (a) rGO bead, (b) rGO-PEDOT hybrid bead, (c) rGO-PEDOT-SiO_2 hybrid bead, (d) surface image of rGO, (e) surface image of rGO-PEDOT hybrid (f) surface image rGO-PEDOT-SiO_2 hybrid (g) cross sectional image of rGO, (h) cross sectional image of rGO-PEDOT hybrid (i) cross sectional image of rGO-PEDOT-SiO_2 hybrid.

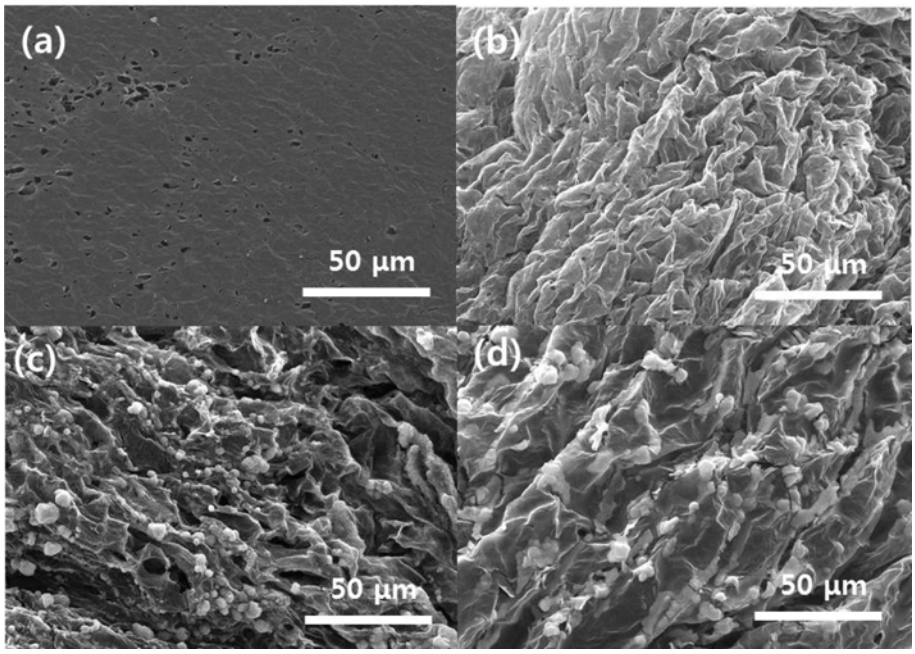

Fig. 5. Surface morphology of changes of rGO-PEDOT-SiO_2 hybrid bead, (a) rGO, (b) rGO-PEDOT-SiO_2 prepared with FTS 10 wt%, (c) rGO-PEDOT-SiO_2 prepared with FTS 20 wt%, (d) rGO-PEDOT-SiO_2 prepared with FTS 30 wt%.

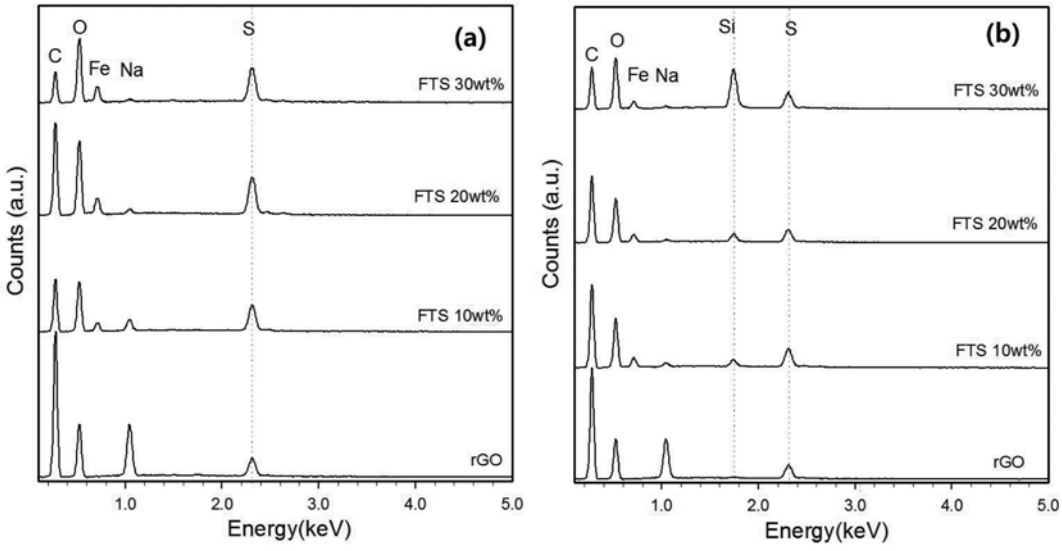

Fig. 6. EDS spectra for various rGO based composite (a) rGO-PEDOT hybrid (b) rGO-PEDOT-SiO_2 hybrid.

tion of rGOA and rGOA-PEDOT or rGOA-PEDOT-SiO_2 composite, such as PEDOT and SiO_2 formation and content (Fig. 6). In the EDS spectrum, the peaks of carbon (C), oxygen (O), iron (Fe), sodium (Na), silicon (Si) and sulfur (S) occurred at 0.28, 0.52, 0.71, 1.04, 1.60 keV, respectively. The element Na in rGOA appeared in SCC when added as a binder during the rGOA spherical particle manufacturing process. The Fe element found in the composite is attributed to the FTS used as the oxidizing agent for VPP, and the FTS, which impregnated the pore, cannot be completely removed in the composite particle during the washing process. The peak of S increased as the PEDOT layer was coated thicker as the oxidizing agent content increases in the rGOA-PEDOT composite (Fig. 6(a)). In addition, in the case of the rGOA-PEDOT-SiO_2 composite, the peaks of the S and Si elements became larger depending on the FTS content. In particular, according to FTS content, the Si peak increases relatively faster than the S peak, which is consistent with the findings of our recent research that TEOS hydration/condensation reaction is faster than EDOT oxidation-coupling reaction [33]. On the other hand, a peak of S was also observed in rGOA, which was presumed to be attributed to the sulfuric acid used in the GO production process produced by Hummer's method. XPS analysis was performed to confirm this assumption. The XPS irradiation spectrum corresponds to Si_{2p} and S_{2p} peaks at around 102 and 165 eV, respectively. In Fig. 7(a), SiO_2 peak at 103.6 eV,

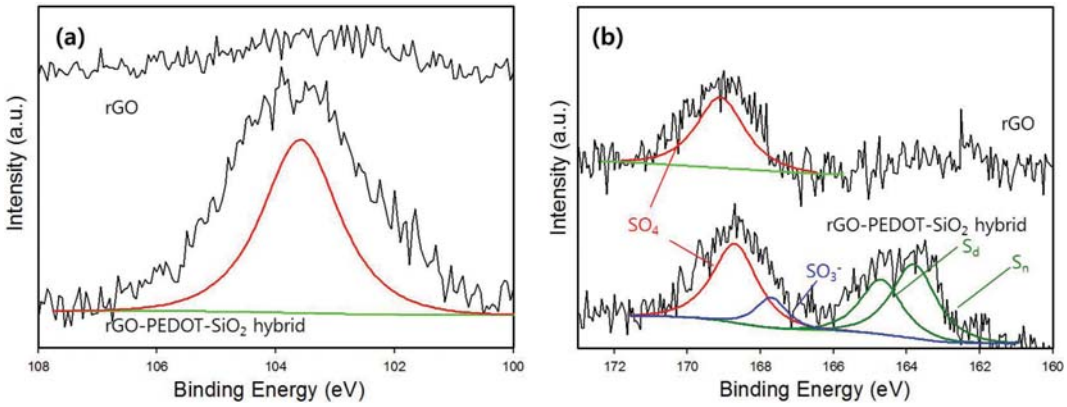

Fig. 7. XPS spectra for various rGO based composite (a) Si_{2p} peak (b) S_{2p} peak.

which was not observed in rGOA due to Si_{2p}, was clearly observed in the rGOA-PEDOT-SiO_2 composite. Fig. 7(b) compares the S_{2p} spectra of the rGOA spherical particles with the rGOA-PEDOT-SiO_2 composite. The peak of 168.9 eV is the same as that of the rGOA spherical particles and the rGOA-PEDOT-SiO_2 composite at the peak of sulfuric acid. The peak at 163.9 eV is the neutral S atom (S_n) peak and 165.6 eV is p-doped S atom (S_d) peak in PEDOT and does not appear in rGO. Likewise, the 167 eV appears when SO_3^- arises from *p*-toluenesulfonic acid, which doped with PEDOT.

2. Electrical Characteristics of rGOA-PEDOT Hybrid Composite

A silver line was deposited on a glass substrate using a thermal evaporator. The hybrid spherical particles were connected to the same contact area using a silver paste to produce a measurement device that is used to investigate the electrical properties of the rGOA-PEDOT-SiO_2 composite (Fig. 8(a)). To verify the minimum lighting voltage of the spherical particles, an LED bulb and wire were connected to the measurement device while raising the voltage of the power supply gradually (Fig. 8(a)). The threshold voltage was 1.4 V when the minimum lighting voltage was confirmed with the rGOA-PEDOT-SiO_2 composite, which was prepared using 10 wt% FTS. After connecting the measuring device to the LCR meter, the resistance value was measured in parallel mode. The resistance of rGOA-PEDOT and rGOA-PEDOT-SiO_2 composites with PEDOT hybrid was lower than that of the measured value for rGO. It is deduced that the PEDOT layer that is present on the surface of the rGOA particle has a high surface area with excellent conductivity. This results in improved contact property at the interface and the resistance value is low. As shown in Fig. 8(c), current density of rGOA-PEDOT-SiO_2 composites with 30 wt% of FTS was much higher than that of rGOA-PEDOT at the same voltage due to microsized bump PEDOT-SiO_2 bump on the surface as shown in Fig. 4(f).

CONCLUSIONS

GOA spherical particles were prepared by freeze casting and thermal reduction, and rGOA-PEDOT or rGOA-PEDOT-SiO_2 composites were successfully prepared *via* SC-VPP process. In the freeze casting process, the radial pore structure developed in the radial direction in the center of the cross section of the rGOA spherical particle due to the temperature gradient of the droplet of the GO aqueous solution. Furthermore, the density of the GO sheet increases toward the center. The morphology of the rGOA-PEDOT-SiO_2 composites prepared using the SC-VPP process remained spherical with the orientation structure of the pores being well developed compared to that of the rGOA-PEDOT composites. In addition, micrometer-sized conductive PEDOT-SiO_2 hybrid spheres are formed on the surface of the rGOA-PEDOT-SiO_2 composite, thereby increasing the contact area with the electrode due to the increase

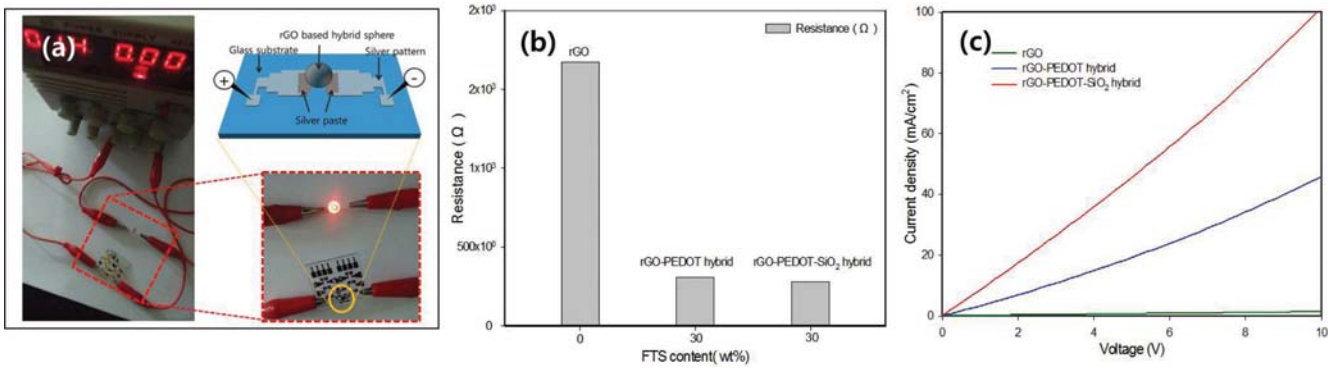

Fig. 8. Comparisons of electrical properties of rGO based composite.

of the surface area of the particle surface. The SC-VPP process proposed in this study can be of good use as a future reference to be applied to various devices requiring control of electrical characteristics.

ACKNOWLEDGEMENTS

This research was supported by the Basic Science Research Program through the National Research Foundation of Korea (NRF) funded by the Ministry of Education (NRF-2016R1D1A3B03931831).

REFERENCES

1. K. S. Novoselov, A. K. Geim, S. V. Morozov, D. Jiang, Y. Zhang, S. V. Dubonos, I. V. Grigorieva and A. A. Firsov, *Science*, **22**, 666 (2004).
2. A. K. Geim and K. S. Novoselov, *Nat. Mater.*, **6**, 183 (2007).
3. W. S. Hummers and R. E. Offeman, *J. Am. Chem. Soc.*, **80**, 1339 (1958).
4. L.-C. Tang, Y.-J. Wa, D. Yan, Y.-B. Pei, L. Zhao, Y.-B. Li, L.-B. Wu, J.-X. Jiang and G.-Q. Lai, *Carbon*, **60**, 16 (2013).
5. A. O'Neill, U. Khan, P. N. Nirmalraj, J. Boland and J. N. Coleman, *J. Phys. Chem. C*, **115**, 5422 (2011).
6. L. Guardia, M. J. Fernández-Merino, J. I. Paredes, P. Solís-Fernández, S. Villar-Rodil, A. Martínez-Alonso and J. M. D. Tascón, *Carbon*, **49**(5), 1653 (2011).
7. Z. Chen, W. Ren, L. Gao, B. Liu, S. Pei and H.-M. Cheng, *Nat. Mater.*, **10**, 424 (2011).
8. M. A. Worsley, P. J. Pauzauskie, T. Y. Olson, J. Biener, J. H. Satcher Jr. and T. F. Baumann, *J. Am. Chem. Soc.*, **132**(40), 14067 (2010).
9. H. Hu, Z. Zhao, W. Wan, Y. Gogotsi and J. Qiu, *Adv. Mater.*, **25**, 2219 (2013).
10. S. Kabiri, D. N. H. Tran, T. Altalhi and D. Losic, *Carbon*, **80**, 523 (2014).
11. S. Bose, T. Kuila, A. K. Mishra, R. Rajasekar, N. H. Kim and J. H. Lee, *J. Mater. Chem.*, **22**, 767 (2012).
12. A. Ouyang, C. Wang, S. Wu, E. Shi, W. Zhao, A. Cao and D. Wu, *ACS Appl. Mater. Inter.*, **7**, 14439 (2015).
13. H. Sun, Z. Xu and C. Gao, *Adv. Mater.*, **25**, 2554 (2013).
14. Y. Zhao, J. Liu, Y. Hu, H. Cheng, C. Hu, C. Jiang, L. Jiang, A. Cao and L. Qu, *Adv. Mater.*, **25**, 591 (2013).
15. Q. Zhou, Y. Li, L. Huang, C. Li and G. Shi, *J. Mater. Chem. A*, **2**, 17489 (2014).
16. C. K. Ching, C. R. Fincher, Y. W. Park, A. J. Heeger, H. Shirakawa, E. J. Louis, S. C. Gau and A. G. MacDiarmid, *Phys. Rev. Lett.*, **39**, 1098 (1977).
17. A. Ouyang, A. Cao, S. Hu, Y. Li, R. Xu, J. Wei, H. Zhu and D. Wu, *ACS Appl. Mater. Inter.*, **8**, 11179 (2016).
18. Y. Wei, J.-M. Yeh, D. Jin, X. Jia, J. Wang, G.-W. Jang, C. Chen and R. W. Gumbs, *Chem. Mater.*, **7**, 969 (1995).
19. A. G. Sommers, *World Patent*, WO 99/58464 (1998).
20. Y.-H. Han, J. Travas-Sejdic, B. Wright and J.-H. Yim, *Macromol. Chem. Phys.*, **212**, 521 (2011).
21. J.-H. Yim, *Compo. Sci. Technol.*, **86**, 45 (2013).
22. R. Khadka and J.-H. Yim, *Macromol. Res.*, **23**, 559 (2015).
23. Y. S. Ko and J.-H. Yim, *Polymer*, **93**, 167 (2016).
24. S. W. Kim, S. W. Lee, J. Kim, J.-H. Yim and K. Y. Cho, *Polymer*, **102** 127 (2016).
25. J. S. Choi, J. S. Park, B. Kim, B.-T. Lee and J.-H. Yim, *Polymer*, **120**, 95 (2017).
26. J. Ahn, S. Yoon, S. G. Jung, J.-H. Yim and K. Y. Cho, *J. Mater. Chem. A.*, **5**, 21214 (2017).
27. J. Lock, S. Im and K. Gleason, *Macromolecules*, **39**, 5326 (2006).
28. S. G. Im and K. K. Gleason, *Macromolecules*, **40**, 6552 (2007).
29. A. Asatekin, M. C. Barr, S. H. Baxamura, K. K. S. Lau, W. Tenhaeff, J. Xu and K. K. Gleason, *Mater. Today*, **13**(5), 26 (2010).
30. S. Deville, E. Saiz, E. R. K. Nalla and A. P. Tomsia, *Science*, **311**, 515 (2006).
31. A. Ouyang and J. Liang, *RSC Adv.*, **4**, 25835 (2014).
32. M. Klotz, I. Amirouche, C. Guizard, C. Viazzi and S. Deville, *Adv. Eng. Mater.*, **14**, 1123 (2012).
33. S. G. Jung, K. Y. Cho and J.-H. Yim, *J. Ind. Eng. Chem.*, **63**, 95 (2018).